Inhibition and Structure of *Trichomonas vaginalis* Purine Nucleoside Phosphorylase with Picomolar Transition State Analogues†

Agnes Rinaldo-Matthis,‡ Corin Wing,‡ Mahmoud Ghanem,‡ Hua Deng,‡ Peng Wu,§ Arti Gupta,§ Peter C. Tyler,|| Gary B. Evans,|| Richard H. Furneaux,|| Steven C. Almo,‡ Ching C. Wang,§ and Vern L. Schramm*,‡

Department of Biochemistry, Albert Einstein College of Medicine, Bronx, New York 10461, Department of Pharmaceutical Chemistry, University of California San Francisco, Mission Bay, Genetech Hall, Suite N572, San Francisco, California 94143-2880, and The Carbohydrate Chemistry Team, Industrial Research, Ltd., New Zealand

Received July 27, 2006; Revised Manuscript Received November 7, 2006

ABSTRACT: *Trichomonas vaginalis* is a parasitic protozoan purine auxotroph possessing a unique purine salvage pathway consisting of a bacterial type purine nucleoside phosphorylase (PNP) and a purine nucleoside kinase. Thus, *T. vaginalis* PNP (TvPNP) functions in the reverse direction relative to the PNPs in other organisms. Immucillin-A (ImmA) and DADMe-Immucillin-A (DADMe-ImmA) are transition state mimics of adenosine with geometric and electrostatic features that resemble early and late transition states of adenosine at the transition state stabilized by TvPNP. ImmA demonstrates slow-onset tight-binding inhibition with TvPNP, to give an equilibrium dissociation constant of 87 pM, an inhibitor release half-time of 17.2 min, and a K_m/K_d ratio of 70,100. DADMe-ImmA resembles a late ribooxacarbenium ion transition state for TvPNP to give a dissociation constant of 30 pM, an inhibitor release half-time of 64 min, and a K_m/K_d ratio of 203,300. The tight binding of DADMe-ImmA supports a late S_N1 transition state. Despite their tight binding to TvPNP, ImmA and DADMe-ImmA are weak inhibitors of human and *P. falciparum* PNPs. The crystal structures of the TvPNP•ImmA•PO_4 and TvPNP•DADMe-ImmA•PO_4 ternary complexes differ from previous structures with substrate analogues. The tight binding with DADMe-ImmA is in part due to a 2.7 Å ionic interaction between a PO_4 oxygen and the N1′ cation of the hydroxypyrrolidine and is weaker in the TvPNP•ImmA•PO_4 structure at 3.5 Å. However, the TvPNP•ImmA•PO_4 structure includes hydrogen bonds between the 2′-hydroxyl and the protein that are not present in TvPNP•DADMe-ImmA•PO_4. These structures explain why DADMe-ImmA binds tighter than ImmA. Immucillin-H is a 12 nM inhibitor of TvPNP but a 56 pM inhibitor of human PNP. And this difference is explained by isotope-edited difference infrared spectroscopy with [6-^{18}O]ImmH to establish that O6 is the keto tautomer in TvPNP•ImmH•PO_4, causing an unfavorable leaving-group interaction.

Trichomonas vaginalis is a highly prevalent protozoan human parasite (*1*) and the causative agent of trichomoniasis (*2*). Although the drug metronidazole is available for the treatment of infections (*3*), it is poorly tolerated, and drug resistance has developed (*4*). Purine salvage is an essential function for all obligate parasitic protozoa (*5*). *T. vaginalis* is unusual in that it lacks a hypoxanthine-guanine phosphoribosyltransferase (HGPRT[1]). Instead, it relies on the nucleoside synthetic reaction of an unusual purine nucleoside phosphorylase (PNP) with broad substrate specificity to form nucleosides that are converted to nucleotides by purine nucleoside kinases (*6*−*8*). The purine auxotrophy of *T. vaginalis* makes PNP an attractive chemotherapeutic target. Adenine, hypoxanthine, and guanine are salvaged to their corresponding nucleosides by PNP and subsequently phosphorylated to form AMP, IMP, and GMP, respectively. PNPs catalyze the reversible phosphorolytic cleavage of the glycosidic bond of purine nucleosides and deoxynucleotides (*9*). PNP from mammalian sources are specific for 6-oxypurines, whereas PNP from certain bacterial and parasitic sources will also use adenine as a substrate (*10*). TvPNP is unusual in having phosphorolytic catalytic activity with inosine, adenosine, and guanosine, thus permitting salvage of all purine bases. Of these, adenine and hypoxanthine are the most favored. A common feature of all known PNPs is the oxacarbenium ion character of the transition state, where cleavage of the C−N bond occurs through an S_N1-like mechanism.

Dissociative transition states can be achieved by following one of several reaction pathways (*10*). The first involves activation of the leaving group, as in the case of acid catalyzed solvolysis of purine nucleosides (*10*). The second occurs as a result of interactions between the catalytic site and the ribosyl moiety to stabilize the oxacarbenium ion charge and geometry (*10*). Other mechanisms involve

† This work was supported by NIH Research Grants GM41916 and AI60660 and the Wenner-Gren Foundation.

* Corresponding author. Tel: (718) 430-2813. Fax: (718) 430-8565. E-mail: vern@aecom.yu.edu.

‡ Albert Einstein College of Medicine.

§ University of California San Francisco.

|| Industrial Research, Ltd.

[1] Abbreviations: DADMe-ImmA, 4′-deaza-1′-aza-2′-deoxy-1′-(9-methylene)-Immucillin-A; ImmA, Immucillin-A; DADMe-ImmH, 4′-deaza-1′-aza-2′-deoxy-1′-(9-methylene)-Immucillin-H; PNP, purine nucleoside phosphorylase; TvPNP, *Trichomonas vaginalis* purine nucleoside phosphorylase; HGPRT, hypoxanthine-guanine phosphoribosyltransferase; pNPR, *p*-nitrophenyl β-D-ribofuranoside.

10.1021/bi061515r CCC: $37.00
Published on Web 12/23/2006

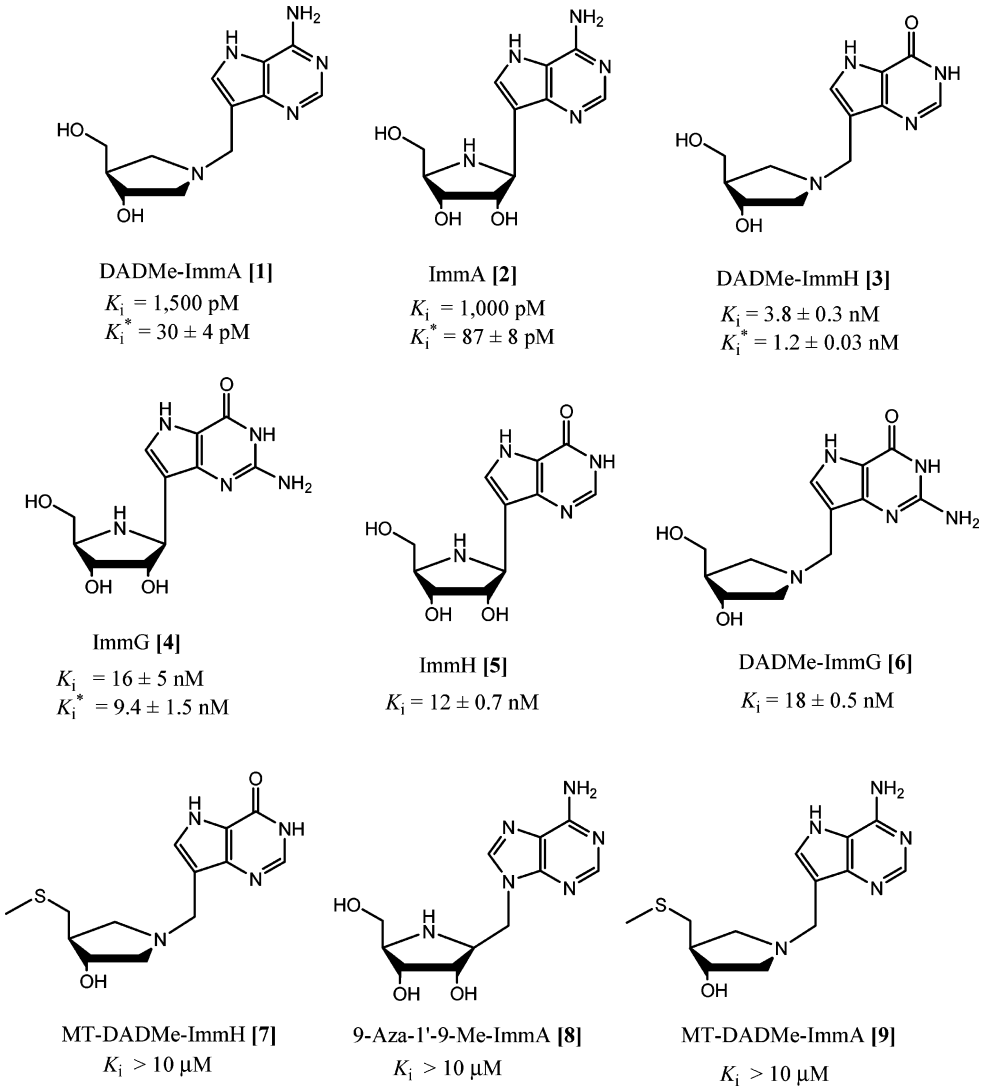

FIGURE 1: Inhibition constants for Immucillins and DADMe-Immucillins as competitive inhibitors of TvPNP. Inhibition constants for the initial rate (K_i) and the slow-onset rate (K_i^*) are indicated when slow onset was observed. When no slow onset occurred, only K_i is given. Compounds indicated with K_i > 10 μM showed no inhibition at 150 μM inhibitor under the assay conditions listed in the Materials and Methods section.

ionization of the 2′-hydroxyl or (3′-hydroxyl) to favor generation of the oxacarbenium ion or activating the attacking phosphate nucleophile (*11*).

p-Nitrophenyl β-D-ribofuranoside (pNPR) can be used as a substrate to distinguish between these mechanisms. If pNPR is a good substrate, catalytic site formation of a ribooxacarbenium ion or activation of the phosphate nucleophile dominate transition state formation. Alternatively, catalytic site ionization of a ribosyl hydroxyl will also facilitate the departure of the *p*-nitrophenolate anion (*12*). If transition state formation is dominated by leaving group activation, involving mono or diprotonation of the purine base, pNPR will be a poor substrate because the *p*-nitrophenylate anion is already active as a leaving group and cannot be further activated by protonation. Because pNPR is an *O*-riboside, protonation of the β-oxygen bridge is also possible but unlikely in an enzyme designed for *N*-riboside phosphorolysis (*13*).

Transition state analogue mimics for mammalian and protozoan PNPs have been synthesized and were shown to have high binding affinities and specificity toward their cognate PNPs (Figure 1). Human and malarial PNPs are specific for 6-oxypurines and Immucillin-H (ImmH) (**5**) and Immucillin-G (ImmG) (**4**) inhibit with dissociation constants in the pM range, but ImmA (**2**) is a poor inhibitor because adenosine is not a substrate for these PNPs (*14*). Adenosine is the primary precursor of the purine salvage pathway in *T. vaginalis* and is a preferred substrate for TvPNP (*15*). We hypothesized that Immucillins based on the structure of adenosine would be powerful inhibitors of TvPNP. The most powerful inhibitors of TvPNP reported previously are adenosine analogues, which include Formycin-A (with a K_i of 2.3 μM; (*16*)) and a subversive substrate 2-fluoro-2′-deoxyadenosine (F-dAdo, with an IC_{50} of 106 nM against *T. vaginalis* in vitro (*3*)). DADMe-Immucillin-A (DADMe-ImmA) (**1**) shows slow-onset, tight-binding inhibition and a remarkable dissociation constant of 30 pM, binding 76,700 times tighter than Formycin-A and 203,300 times tighter than adenosine.

The structures of TvPNP·DADMe-ImmA·PO_4 and TvPNP·ImmA·PO_4 show that the carboxyl group of Asp204 hydrogen bonds to N7H and N6H of the 9-deazaadenine base with distances of 3.0 and 2.8 Å, respectively. Other TvPNP inhibitor complexes have Asp204 pointing away from the base or have interactions that are significantly weaker (*3*).

Phosphate is held tightly in the TvPNP·DADMe-ImmA·PO_4 complex and forms a close ion pair between the incipient phosphate nucleophile and the N1′ cation of bound DADMe-ImmA. In the ImmA complex, the ion pair is weaker. Thus, leaving group interactions and an ion pair mimic of the transition state provide the binding energy for the Immucillins.

MATERIALS AND METHODS

TvPNP Assay. TvPNP was prepared as described earlier (*3*). The inosine phosphorolytic activity of TvPNP was monitored by following the conversion of hypoxanthine to uric acid ($\epsilon_{293} = 12.9$ mM^{-1} cm^{-1}) (*17*) at 25 °C in a coupled assay containing 60 milliunits of xanthine oxidase, variable inosine concentrations (1 μM to 3 mM) in a final volume of 1 mL of 50 mM KH_2PO_4 at pH 7.4. The hydrolysis of pNPR was observed by the liberation of *p*-nitrophenol ($\epsilon_{405} = 12.5$ mM^{-1} cm^{-1}) in 50 mM KH_2PO_4 at pH 7.4. The reactions were initiated by the addition of enzyme, typically at 2 nM final concentration.

Slow-Onset Inhibition. The slow onset of inhibition was measured following the addition of enzyme to complete assay mixtures at 1 mM inosine and various inhibitor concentrations (*18*). Inhibitor concentrations were determined spectrophotometrically using the published millimolar extinction coefficients of 8.5 at 275 nm, 9.54 at 261 nm, and 8.92 at 269 nm at pH 7 for 9-deazaadenosine (ImmA based inhibitors), 9-deazainosine (ImmH based inhibitors), and 9-deazaguanosine (ImmG based inhibitors), respectively (*19*, *20*). Enzyme (0.5−5 nM final concentration) was added to assay mixtures followed by monitoring of product formation. Rates were monitored for 1−2 h to determine both the initial reaction rate and to determine if a second reaction rate occurred as a result of slow-onset inhibition. The inhibition constant (K_i) for the initial rate was determined from its fit to eq 1, which describes the competitive inhibition pattern of the Immucillin based inhibitors (*Imm*) and inosine as substrate (*A*). K_m is the Michaelis constant for inosine (*A*), K_i is the dissociation constant for inhibitor with the TvPNP·PO_4 complex, assuming competitive inhibition. The dissociation constant for the equilibrium complex after slow-onset inhibition has occurred, K_i^{*}[2], was determined from fits of the final slopes to eq 1. This analysis is only valid when enzyme concentration is 10-fold less than inhibitor concentration. When the enzyme concentration is significant, it depletes the free inhibitor, and the effective inhibitor concentration can be corrected by the expression: $I_{free} = I_{total} - (1 - v_s/v_o)E_t$, where I_{free} is the free inhibitor concentration, I_{total} is the total added inhibitor, v_s is the steady-state inhibited catalytic rate, v_o is the uninhibited catalytic rate, and E_t is the total enzyme concentration.

$$\frac{v}{e} = \frac{k_{cat}A}{K_m\left[1 + \left(\frac{Imm}{K_i}\right)\right] + A} \quad (1)$$

Immucillin Off Rates. A time-dependent dissociation is expected for the bound inhibitor following dilution of the enzyme−inhibitor complex into assay mixtures with no inhibitor (*20*). The tightly bound E^{*}·I·PO_4 complex was formed by incubation of 40 μM enzyme subunits with 34 μM inhibitor in 50 mM phosphate buffer at pH 7.4, a condition known to saturate one-third of the catalytic sites and to cause full inhibition under conditions where most of the inhibitor is bound to the enzyme (*20*). Rapid serial dilution of the E^{*}·I·PO_4 complex into buffer (1:200) followed by dilution into the assay mixture (1:200) demonstrated time-dependent release of the inhibitor (*20*). At high concentrations of inosine (5 mM) as the substrate, the rate of activity regain can be used to estimate k_3 and k_4[2]. The rate k_4 is estimated by fitting absorbance at 293 nm (*P*) versus time (*t*) to the equation: $P = v_s t + (v_o - v_s)(1 - e^{-kt})/k$, where v_s is the rate at time zero, v_o is the rate at time *t*, and $k = k_4$. The rate of activity regain can also be used to estimate k_3[2].

Crystallization of TvPNP−Immucillin-A Complexes. TvPNP in 50 mM Hepes at pH 7.2 containing 2 mM DTT and 2 mM $MgCl_2$ was concentrated to 8 mg/mL and incubated on ice for 10 min with 1 mM Immucillin-A (**2**) or 1 mM DADMe-ImmA (**1**) and 1 mM KH_2PO_4. The TvPNP·ImmA·PO_4 complex was crystallized by hanging drop vapor diffusion at 18 °C using 80 μL of reservoir solution containing 0.2 M lithium citrate and 20% (w/v) PEG3350 at pH 8.5. The TvPNP·DADMe-ImmA·PO_4 complex was crystallized using the same technique but with 0.17 M sodium acetate, 0.085 M Tris-HCL at pH 8.8, 25.5% PEG 4000, and 15% glycerol as the reservoir solution.

Data Collection. Crystals were soaked in mother liquor supplemented with 20% glycerol and flash cooled to −178 °C prior to data collection. Diffraction from the TvPNP·ImmA·PO_4 crystals was consistent with the space group $P6_2$ ($a = b = 155$ and $c = 102$ Å) with three molecules in the asymmetric unit. The Matthews coefficient was 4.5 $Å^3$/Da, which corresponds to a solvent content of 72%. The TvPNP·DADMe-ImmA·PO_4 complex exhibited diffraction consistent with the space group $P2_12_12_1$ ($a = 82$, $b = 114$ and $c = 195$ Å) with six molecules in the asymmetric unit. The Matthews coefficient was 2.96 $Å^3$/Da, which corresponds to a solvent content of 58%. Diffraction data were collected to a resolution of 2.7 Å for both complexes at beamline X29A at the National Synchrotron Light Source, Brookhaven National Laboratory using an ADSC Quantum 315 detector. Each frame was exposed for 10 s with an oscillation range of 1°. The HKL2000 suite (*21*) was used for integration and scaling of the data (Table 1).

Structure Determination and Refinement. The structure of TvPNP in complex with ImmA (**2**), DADMe-ImmA (**1**), and PO_4^{2-} was solved by molecular replacement using the monomeric form of TvPNP (Protein Data Bank ID code 1Z33.pdb without water) as a search model. Molecular replacement with MOLREP (*22*), and refinement with REFMAC5 (*23*) were performed with the CCP4i package (*24*). COOT (*25*) was used for molecular modeling. Weak NCS restraints were applied in the initial stages of refinement

[2] Origin of K_i and K_i^{*} based on the slow-onset tight-binding of immucillins: TvPNP·OP_4 + Imm $\underset{k_2}{\overset{k_1}{\rightleftharpoons}}$ TvPNP*·Imm·PO_4 $\underset{k_4}{\overset{k_3}{\rightleftharpoons}}$ TvPNP*·Imm·PO_4

[3] $K_i = k_2/k_1$

[4] $K_i^{*} = K_i k_4/(k_3 + k_4)$

Table 1: Data Processing and Refinement Statistics

	TvPNP-ImmA	TvPNP-DADMe-ImmA
wavelength (Å)	0.979301	0.979099
resolution (Å)	2.7	2.7
unique reflections	37032	50207
completeness (%)[a]	99.3 (99.5)	98.1 (93.8)
multiplicity	6.2	6.9
R_{sym} (%)[a,b]	6.9 (41.8)	11.6 (59.4)
I/σ[a]	17 (3)	11.4 (1.7)
no. of protein atoms	5242	10721
no. of water molecules	73	170
R-factor	17.0	19.9
R_{free}	22.5	25.1
average *B*-factor	60	37.8
r.m.s bond (Å)	0.02	0.01
r.m.s angle (Å)	1.5	1.3
Ramachandran analysis		
most favored	83.5%	84.5%
allowed	16.0%	15.2%
disallowed	0.5%	0.3%

[a] The values for the highest resolution shell are given in parentheses. [b] $R_{sym} = (\Sigma_{hkl}\Sigma_i|I_i(hkl) - \langle I(hkl)\rangle|)/\Sigma_{hkl}\Sigma_i I_i(hkl)$ for *n* independent reflections, and observations of a given reflection, $\langle I(hkl)\rangle$, is the average intensity of the *i* observation.

to improve the maps and removed in the later stages. Clear ligand density was observed in the *F*o − *F*c maps contured at 5σ.

In the TvPNP·ImmA·PO_4 complex, residues 206−223 were not well resolved in two of the three monomers in the asymmetric unit (A and C), and these residues were not included in the final model of the TvPNP·ImmA complex. However, interpretable electron density was present for this loop region in the third monomer (B). After the protein and ligands were refined, water molecules were included in the structure. The final structure had *R*-factor and R_{free} values of 17.0% and 22.5%, respectively.

The six independent molecules in the TvPNP·DADMe-ImmA·PO_4 structure also lacked density for the loop region missing in the TvPNP·ImmA·PO_4 complex. The *C*-terminal His tag was partially built in monomers A, B, C, D, and F. The final structure of the DADMe·ImmA·PO_4 complex had an *R*-factor of 19.9% with an *R*-free value of 25.5%. All Figures were created using PYMOL (*26*).

[6-^{18}O]ImmH Binding in the TvPNP Complex. Free TvPNP was concentrated to 3 mM against 0.2 M NaCl using a 0.5 mL 10 K molecular weight retention centrifugal filter (Millipore). [6-^{18}O]ImmH (**1**) and phosphate buffer at pH 7.4, both at 3 mM were incubated with TvPNP. The free inhibitor and phosphate were washed away with 0.2 M NaCl in order to generate a 3 mM TvPNP·[6-^{18}O]ImmH·PO_4 complex for IR studies. The same procedure was used in matched samples to generate the same complex with [6-^{16}O]-ImmH. FTIR spectroscopy was performed on a Magna 760 Fourier transform spectrometer (Nicolet Instrument Corp., WI) using a MCT detector. A CaF_2 window with a 25 μm Teflon spacer was used. Spectra were collected in the range of 900−4000 cm^{-1} with 2 cm^{-1} resolution. A Blackman−Harris three-term apodization and a Happ−Genzel apodization were applied. Omnic 4.1a (Nicolet Instruments, Corp.) software was used for data collection and analysis.

Table 2: Kinetic Constants for TvPNP with Various Substrates

substrate	K_m (μM)	k_{cat} (s^{-1})	k_{cat}/K_m (M^{-1} s^{-1})
adenosine	6.1 ± 0.5	1.7 ± 0.2	2.8×10^5
guanosine	60 ± 8	1.1 ± 0.1	1.8×10^4
inosine	25 ± 1	1.8 ± 0.1	7.2×10^4
pNPR	90 ± 42	$1.0 \pm 0.1 \times 10^{-3}$	1.1

Table 3: Inhibition Constants (K_i and K_i^*) for Immucillin Based Inhibitors of TvPNP

inhibitor	K_i (pM)	K_i^* (pM)
DADMe-Immucillin-A (**1**)	1500 ± 130	30 ± 4
Immucillin-A (**2**)	1000 ± 90	87 ± 8
DADMe-Immucillin-H (**3**)	3800 ± 300	1200 ± 30
Immucillin-G (**4**)	16,000 ± 5,000	9400 ± 1500
Immucillin-H (**5**)	12,000 ± 700	na[a]
DADMe-Immucillin-G (**6**)	18,000 ± 500	na[a]
MT-DADMe-Immucillin-H (**7**)	>10,000,000	na[a]
9-Aza-1′-9-Me-Immucillin-A (**8**)	>10,000,000	na[a]
MT-DADMe-Immucillin-A (**9**)	>10,000,000	na[a]

[a] No slow onset observed.

RESULTS AND DISCUSSION

Substrate Specificity of TvPNP. Adenosine is the preferred substrate for the phosphorolysis reaction of TvPNP with a catalytic efficiency of 2.8×10^5 M^{-1} s^{-1} and a relatively low K_m of 6.1 μM (Table 2). Inosine has higher k_{cat} and K_m values for a similar k_{cat}/K_m of 7.2×10^4 M^{-1} s^{-1}. The enzyme is less efficient with guanosine as a substrate by approximately an order of magnitude. Ribooxacarbenium ion stabilization by ribohydrolases can be tested by ribosyl derivatives with good leaving groups, and pNPR has been used for this purpose (*10*). TvPNP had a K_m of 90 μM and a k_{cat} of 10^{-4} s^{-1} for pNPR (Table 2) to give a k_{cat}/K_m for this compound of 1.1. This is 2.5×10^5 fold lower than the k_{cat}/K_m for TvPNP with adenosine (*16*). Catalytic efficiency of TvPNP for adenosine is similar to that observed for bovine and human PNPs with inosine, although the mammalian enzymes do not accept adenosine as a substrate. pNPR is also a poor substrate for bovine PNP with a k_{cat}/K_m of 0.89 M^{-1} s^{-1} (*10*) similar to the catalytic efficiency with TvPNP. Human PNP had no significant activity with pNPR (level of detection was <0.1 M^{-1} s^{-1}, result not shown). Poor substrate function for pNPR suggests a strong requirement for leaving group activation for both mammalian PNPs and TvPNP. Protonation at the N1 and N7 nitrogens of the purine ring and hydrogen-bonds to the 6-exocyclic oxygen are established mechanisms for the activation of inosine/hypoxanthine in mammalian PNPs. Specifically, Glu201 of the mammalian PNP interacts at N1, and Asp243 spans a protonated N7H and O6 for transition state stabilization in complexes with Immucillin-H (**5**). These interactions differ in TvPNP, where Asp204 replaces Asn243. In order to accept both adenine and hypoxanthine bases for efficient catalysis in TvPNP, it is likely that the protonation pattern of the carboxylate changes to accommodate the change of H-bond donor/acceptor at C6 (from amino in adenine to a carbonyl oxygen in hypoxanthine).

Slow-Onset Inhibition of TvPNP. Immucillin-A (**2**) is a slow-onset tight-binding transition state analogue, with a K_i of 1,000 pM and a K_i^* of 87 pM (Table 3 and Figure 1). In contrast, ImmA binds to the *P. falciparum* and human PNPs

with K_i* values of greater than 10 μM (*27*) and 2.6 μM for bovine PNP (*28*). DADMe-ImmA (**1**) is a more powerful inhibitor of TvPNP and binds tightly with a K_i^* of 30 pM. Some hexameric PNPs, like that from *Plasmodium falciparum* use 5′-methylthioinosine as substrates (*29*). In those cases, 5′-methylthio-substituted Immucillins are powerful inhibitors (*14*). For TvPNP, MT-DADMe-ImmA **[9]** has a dissociation constant >200,000 times that for DADMe-ImmA; thus, the 5′-methylthio group prevents binding (Figure 1). Because TvPNP does not accept 5′-methylthio groups, it is unlikely to be involved in 5′-methylthioadenosine metabolism in *T. vaginalis*. ImmG (**4**) has a dissociation constant of 42 pM for trimeric human PNP and 900 pM for hexameric *P. falciparum* PNP, and relatively weak binding to TvPNP ($K_i^* = 9.4$ nM). DADMe-ImmG (**6**) is a powerful inhibitor of human PNP with a K_i^* of 7 pM; however, the K_i^* for TvPNP is 18 nM. TvPNP, with its preference for adenosine, prefers DADMe-ImmA as a picomolar transition state analogue, whereas human PNP, with deoxyguanosine as a critical substrate, prefers DADMe-ImmG as a transition state analogue.

ImmH (**5**) binds to TvPNP with a K_i of 12 nM, a greatly reduced affinity relative to human and bovine PNPs (dissociation constants of 56 and 23 pM, respectively). DADMe-ImmH (**3**) has a dissociation constant of 1.2 nM for TvPNP, an affinity decreased by 40-fold relative to DADMe-ImmA (**1**) (*5*). The relatively tight binding of both inosine and adenosine transition state mimics to TvPNP distinguishes this enzyme from all previously reported PNPs. Leaving group interactions at PNP catalytic sites are usually specific for 6-amino or 6-oxy substituents, but TvPNP accepts both, and this broad specificity is reflected in its transition state analogue specificity. DADMe-ImmA (**1**) (*5*) binds 2.2 kcal/mol more favorably than DADMe-ImmH (**3**) (*2*). This difference reflects interactions of the 6-amino and 6-carbonyl groups of the Immucillins at the catalytic site and is characterized by the structural and spectroscopic analyses described below.

Rate Constants for Interaction of DADMe-ImmA and ImmA. Slow-onset tight-binding inhibitors interact through rapid, weak interactions followed by an inhibitor-induced conformational change that causes tight binding (Figure 2). For TvPNP inhibition by DADMe-ImmA (**1**), a short-lived ($t_{1/2}$ of 79 s) initial interaction with a 1,500 pM K_i is followed by slow-onset inhibition. The affinity increases 50-fold to give a K_i* of 30 pM after the slow-onset step has equilibrated (after 60 min). The slow-onset inhibition pattern with ImmA (**2**) is similar, and the binding equilibrium gives a K_i* of 87 pM (Figure 2). The dilution of inhibited enzyme into excess substrate gave an inhibitor $t_{1/2}$ off-rate of 17.2 min for ImmA (**2**) and 64 min for DADMe-ImmA (**1**) (Table 4). In comparison, this rate is 72 min for the 23 pM interaction of ImmH (**5**) with bovine PNP (*20*).

Crystal Structure of TvPNP·ImmA·PO₄ and the TvPNP·DADMe-ImmA·PO₄. The structures of TvPNP·ImmA·PO_4 and TvPNP·DADMe-ImmA·PO_4 were determined by X-ray crystallography for comparison of the structures of other inhibitors (*3*). The TvPNP·ImmA·PO_4 structure has 3 monomers in the asymmetric unit. The application of a crystallographic 2-fold axis generates the functional hexameric structure, which is a trimer of dimers (Figure 3a). The six active sites are composed of residues contributed by a pair of monomers. Each monomer of TvPNP has a β-sheet core flanked by seven α-helices. The TvPNP·DADMe-ImmA·PO_4 structure has six monomers in the asymmetric unit, which correspond to the functional hexamer. The

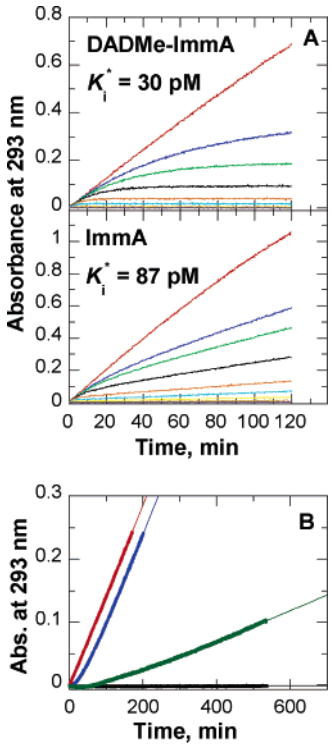

FIGURE 2: Immucillin binding to and release from TvPNP. (A) Slow-onset inhibition of TvPNP with various concentrations of DADMe-Immucillin-A (**1**) (upper panel) and Immucillin-A (**2**) (lower panel) in 50 mM KH_2PO_4 at pH 7.4 at 25 °C. The reactions were initiated by the addition of enzyme (~5 nM) into 1 mL reactions mixtures containing 1 mM inosine as the substrate, 60 milliunits of xanthine oxidase, and varied inhibitor concentrations. In the upper panel (A), DADMe-ImmA concentrations are 0 (red), 8 nM (blue), 16 nM (green), 32 nM (black), 80 nM (orange), 160 nM (cyan), 400 nM (yellow), 800 nM (brown), and 1600 nM (purple). In the lower panel (A), ImmA concentrations are 0 (red), 6.6 nM (blue), 13.2 nM (green), 26.4 nM (black), 66 nM (orange), 132 nM (cyan), 330 nM (yellow), 660 nM (brown), and 1,320 nM (purple). Gray curves are negative controls with no enzyme. The UV changes at 293 nm due to the formation of uric acid were monitored for 120 min in the coupled xanthine oxidase assays. (B) Dissociation of ImmA (blue curve) and DADMe-ImmA (green curve) from TvPNP. The enzyme (40 μM) and Immucillins (34 μM) were incubated for 1 h at 30 °C, followed by 40,000-fold dilution into xanthine oxidase coupling assay mixtures containing 5 mM of inosine and 50 mM KH_2PO_4 at pH 7.4. In the positive control assay (red curve), an equivalent enzyme sample was treated in the same manner except that incubation was with the buffer. The background (black curve) shows the spectrophotometer response when no PNP is added to the reaction mixture. Data were fit to the equation for regain of enzyme activity as indicated in the Materials and Methods section.

Table 4: Immucillin Binding and Release Constants

constant	ImmA	DADMe-ImmA
K_i	1000 pM	1500 pM
K_i^*	87 pM	30 pM
k_3[a]	7.0×10^{-3} s^{-1}	8.8×10^{-3} s^{-1}
k_4[b]	$6.7 \pm 1.0 \times 10^{-4}$ s^{-1}	$1.8 \pm 0.5 \times 10^{-4}$ s^{-1}
$t_{1/2}$ on	99 s	79 s
$t_{1/2}$ off	17.2 min	64 min

[a] The values of k_3 were estimated using K_i, K_i^*, and k_4 (see footnote 2). [b] The values of k_4 were determined experimentally from Figure 2B.

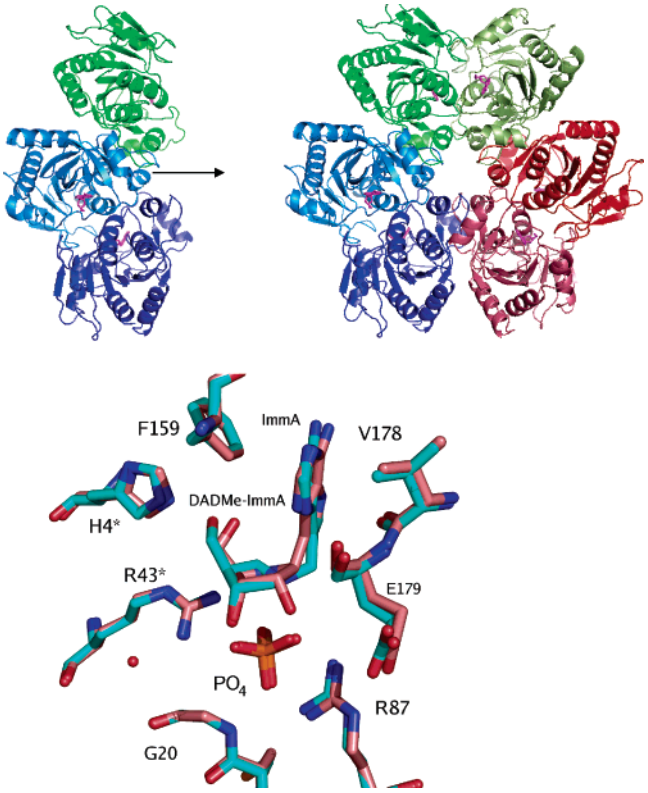

FIGURE 3: X-ray crystal structure of TvPNP with ImmA (**2**) and PO_4 bound in the active site. Molecules in the asymmetric unit generate the hexamer by applying 2-fold crystallographic symmetry (upper panel). Each pair of monomers is represented with similar colors. The crystal structure of TvPNP in complex with DADMe-ImmA and PO_4 bound in the active sites was solved with a hexamer in the asymmeric unit. The lower panel provides superpositions of the Immucillins at the active sites of the two TvPNP structures. The complex with ImmA (**2**) is shown in pink, and the complex with DADMe-ImmA (**1**) is shown in cyan.

structures with bound Immucillins are similar to TvPNP without ligands at the catalytic site (1Z33.pdb) and to *E. coli* PNP in complex with 2-F-adenosine and phosphate (1PK9.pdb) but also reveal differences as discussed below (*3*, *30*).

Active Site of TvPNP. The structures of TvPNP·ImmA·PO_4 and TvPNP·DADMe-ImmA·PO_4 show the active site located at the interface between each pair of monomers. Clear electron density was observed for the inhibitor and for the bound phosphate. The ligands in monomers A and C in the ImmA·PO_4 complex have higher *B*-factors (80 Å^2) than those in monomer B (60 Å^2), suggesting slightly higher ligand occupancy or structural order in monomer B compared to monomers A and C. The three dimers of the hexamer in the asymmetric unit of the TvPNP·DADMe-ImmA·PO_4 complex show *B*-factor patterns similar to those of the ImmA complex. Differential *B*-factors may relate to crystallographic differences or the negative cooperativity known to be induced by inhibitor binding in mammalian PNPs (*20*).

The two TvPNP−Immucillin-A complexes are similar to each other and superimpose well with a rms deviation of 0.3 Å, comparing 236 residues (Figure 3, lower panel). The active site can be divided into the purine base binding site, the sugar binding site, and the phosphate binding site. The purine base is surrounded by four hydrophobic residues Phe159, Val178, Met180, and Ile206, where Phe159 and Val178 form hydrophobic interactions with the base (Figures 4a). The side chains of Ile206 and Met180 form hydrophobic van der Waals interactions near the 6-amino group and the N3 of the 9-deazaadenine ring of bound ImmA and DADMe-ImmA.

N1 of the deazapurine base accepts a hydrogen bond from a structurally conserved water that also hydrogen bonds to the carbonyl oxygen of Phe159 (distances of 2.7−2.9 Å). OD2 and OD1 of the catalytically important Asp204 form hydrogen bond interactions with N7 and N6 of the base with distances of 2.7 and 3.0 Å, respectively (Figure 5). The close interaction of Asp204 and the base suggests the formation of the transition state by Asp204 acting as the general acid proton donor to N7 of the adenine leaving group. Proton donation from Asp204 to form the transition state requires that Asp204 be protonated prior to reaching the transition state. Thus, the pK_a of this group, prior to transition state formation, must have a sufficiently high pK_a to permit the formation of acidic Asp204 at neutral pH.

The ribose sugar is recognized by His4* (* indicates a contact from the adjacent subunit), Glu181, and Thr90. The 5′-OH group of the sugar forms hydrogen bonds with NE2 of His4* (2.6−3.2 Å). The O2′ and O3′ of the sugar participate in several hydrogen bonds with OE1 and OE2 of Glu181 (2.6 and 2.6 Å) and with O1 and O3 of the phosphate group (2.5 and 3.1 Å) in the TvPNP−ImmA complex. DADMe-ImmA lacks the O2′ group and is missing the hydrogen bonds associated with this group (Figure 5). Instead, the N1′ of the ribose ring participates in a 2.7 Å ion pair with the O3 of the phosphate group. Ion pair formation in a relatively hydrophobic catalytic site contributes to the high affinity of DADMe-ImmA for TvPNP.

The anionic phosphate binding site contains cations contributed by Arg24, Arg87, and Arg43* and H-bond donors from the main chain amino group of Gly20. Another cation is provided by bound Immucillins. For ImmA, the cationic imino nitrogen N4′ of ImmA is near the phosphate, as is the N1′ cation from bound DADMe-ImmA. The PO_4 moiety O2 also hydrogen bonds with the carbonyl oxygen of Thr90, whereas O3 and O1 interact with the 2′-OH (3.1 Å) and 3′-OH (2.5 Å) of ImmA, respectively. Phosphate O2 forms hydrogen bond or ion pair interactions with NH2 of Arg24 (2.8 Å), NH2 of Arg43* (2.7 Å), and OG1 of Thr90 (2.7−2.9 Å). Phosphate O4 interacts with NH1 of Arg24 (3.0 Å) and the amino group of Gly20 (2.6 Å). Phosphate O3 interacts with the NH2 of Arg87 (2.7−3.0 Å), the amino group of Thr90 (3.0−3.2 Å), and the N4′ cation of ImmA (3.1 Å). The N1′ of the carbocation in the DADMe-ImmA complex forms an ion pair with the same oxygen of the PO_4 (2.9 Å). The apparent nucleophilic oxygen is O3 of the phosphate, and the distance between the nucleophile, C1′, and the cationic N4′ of the ImmA is 3.4 and 3.1 Å, respectively. DADMe-ImmA has a 2.9 Å distance between the ribocation mimic and the 9-deazaadenine leaving group to resemble the geometry of a fully developed S_N1 transition state. Transition state analysis of human, bovine, and *P. falciparum* PNPs have placed the attacking phosphate oxygen nucleophile approximately 3.0 Å from the C1′ carbocation at these transition states (*31*, *32*). The 3.0 Å distance between N4′ of bound ImmA and the anionic O3 of phosphate provides both geometric and ionic mimicry of these transition states. However, when the ImmA transition state analogue is bound, its N4′ cation is slightly more distant, and the

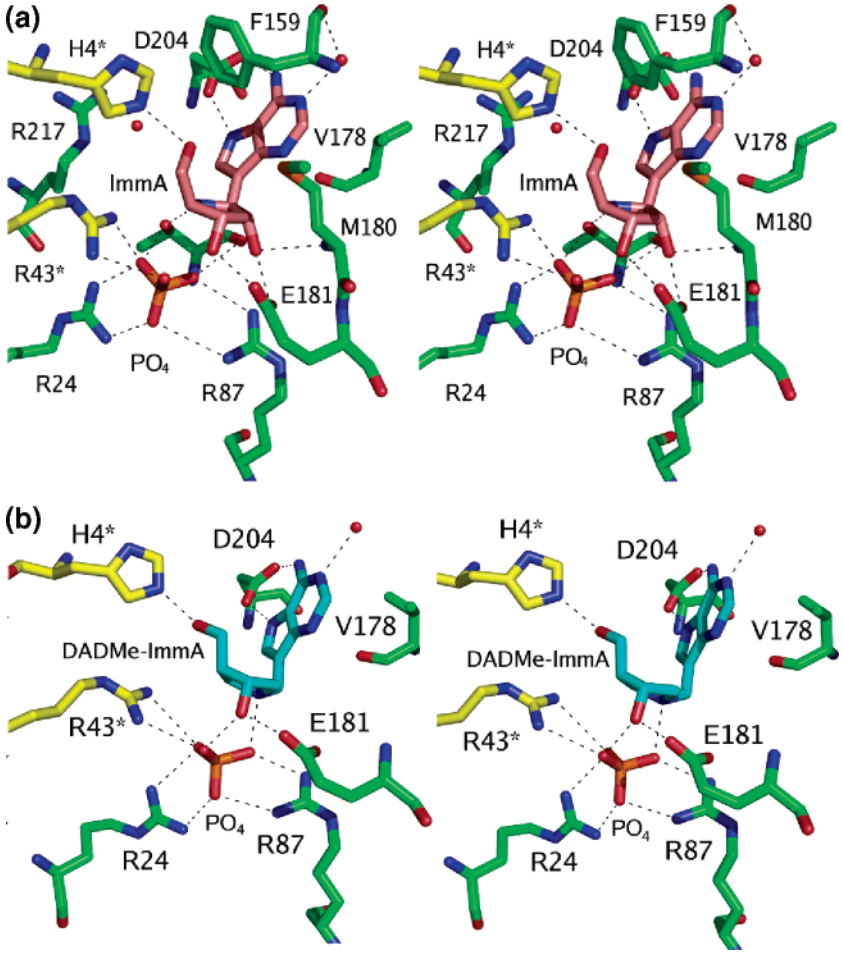

FIGURE 4: Stereoviews of the catalytic site contacts in TvPNP with the transition state analogue inhibitors ImmA (**2**) and DADMe-ImmA (**1**) and PO_4 in the catalytic sites. (a) Stereoview of the active site of TvPNP in complex with ImmA, and PO_4 is shown and is compared in (b) to the stereoview of the active site of TvPNP in complex with DADMe-ImmA and PO_4.

cationic charge is moved from the position of the cation in the actual transition state.

Comparison of TvPNP·ImmA·PO₄ with Homologous Structures. The catalytic mechanism proposed for TvPNP involves Asp204 as the proton donor to N7 of the leaving group. In the crystal structure of TvPNP·ImmA·PO_4, Asp204 accepts hydrogen bonds from $NH_2$6 and NH7 of the ImmA base. In the DADMe-ImmA complex, these hydrogen bonds are even shorter, in agreement with its tighter binding. Most previously reported TvPNP complexes (*3*, *27*) have Asp204 pointing away from the base (Figure 6). Only TvPNP in complex with Formycin-A (1z36.pdb) (*3*) has Asp204 in the proposed active conformation with hydrogen bonds with the N7 and $NH_2$6 of the base, similar to Immucillin interactions (Figure 6, 7). Formycin-A is a 2.3 μM inhibitor of TvPNP, and the interactions with Asp204 in the TvPNP·Formycin·A structure (*3*) are weaker (3.4 and 3.2 Å, respectively) than those seen in the TvPNP·ImmA·PO_4 structure (3.0 and 2.8 Å, respectively) and in the DADMe-ImmA complex (2.9 and 2.7 Å, respectively). Although these are close to the limits of experimental uncertainty, distances systematically become shorter with the more tightly bound inhibitors. The favorable hydrogen bonds between NH7 and $NH_2$6 and Asp204 with bound ImmA or DADMe-ImmA support transition state stabilization of adenosine by these interactions.

ImmH Binding in the TvPNP Complex. The promiscuous nature of TvPNP with regards to inosine, guanosine, and adenosine substrate specificity led us to the hypothesis that a 6-enol tautomer of inosine and guanosine might be required for catalysis. Protonated Asp204 donates its proton to N7 at the transition state of these substrates. Therefore, the carbonyl oxygen (═O) would form an unfavorable interaction with O6, unless it exists at the enol (−OH) form. Then, favorable interactions could occur at both N7 and O6. This hypothesis was tested by the binding of ImmH to form TvPNP·ImmH. The IR difference spectrum between the TvPNP·ImmH and TvPNP·[6-^{18}O]ImmH complexes (Figure 5) contains only vibrational modes from [6-^{16}O/6-^{18}O]ImmH when bound to TvPNP. The positive bands are due to [6-^{16}O]ImmH, and the negative bands are a feature of [6-^{18}O]ImmH. The observation of a C6═O stretch frequency at 1672 cm^{-1} in the ImmH·TvPNP complex suggests that bound ImmH exists primarily in the keto form. The positive peak in the difference spectra is shifted from 1667 to 1672 cm^{-1} (a difference of +6) in the TvPNP·ImmH complex. This frequency change indicates a weaker H bond between the enzyme and C6═O when ImmH is bound to TvPNP than when it is in solution. In contrast, the binding of ImmH in the complex of human PNP and PO_4 reveals a stronger H bond to C6═O but not the enol form (not shown). The relatively weak binding interaction (K_i = 12 nM) seen between ImmH and TvPNP is 138-fold weaker (3.0 kcal/mol) than that for ImmA, consistent with the loss of one H bond between the exocyclic group at C6 and Asp204.

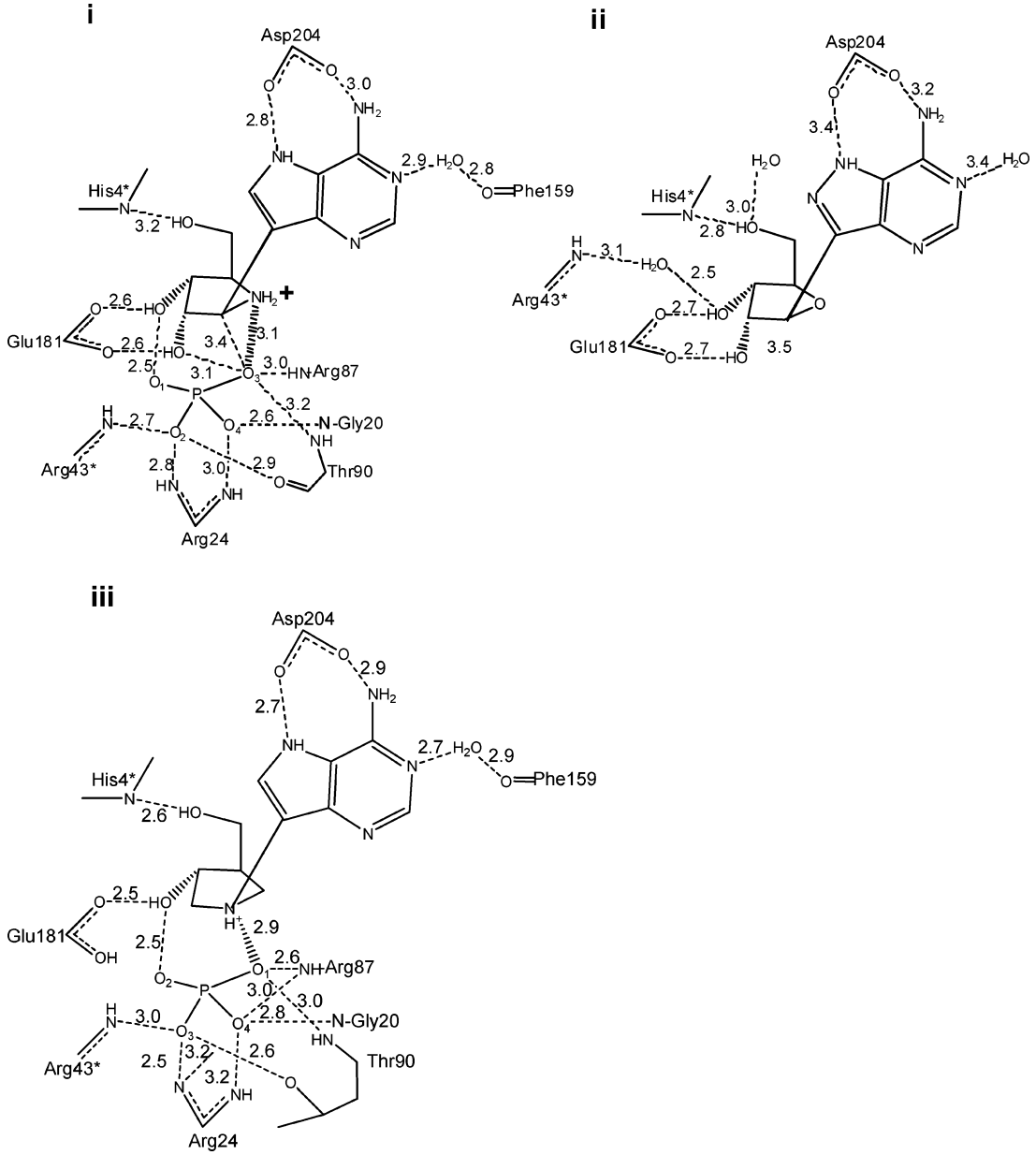

FIGURE 5: Distance maps of (i) TvPNP·ImmA·PO_4 compared to (ii) TvPNP· Formycin-A (from 1z36.pdb, ref 3 (*3*)) and (iii) TvPNP·DADMe-ImmA·PO_4.

CONCLUSIONS

The adenosine transition state analogue DADMe-ImmA (**1**) resembles a fully dissociated adenosyl ribocation transition state and is a powerful, slow-onset tight-binding inhibitor for TvPNP with a K_i* value of 30 pM and a K_m/K_i* value of 203,300. Immucillin-A (**2**) resembles an early S_N1 transition state with adenosine partly dissociated at the *N*-ribosidic bond and binds with a dissociation constant of 87 pM. This inhibition pattern suggests that TvPNP forms a fully dissociated transition state for the phosphorolysis of adenosine. The 6-amino group is important to transition state analogue binding because DADMe-ImmH (**3**) and ImmH (**5**) bind with dissociation constants of 1.2 and 12 nM, respectively. In contrast, human, bovine, and *P. falciparum* PNPs bind ImmH (**5**) with dissociation constants of 56, 23, and 860 pM, respectively. The interaction of DADMe-ImmA (**1**) with TvPNP is the tightest-binding enzymatic interaction known for an Immucillin analogue of adenosine. The relative affinity for Immucillins and DADMe-Immucillins has been shown to be a dependable indication of early and late dissociative (S_N1) transition states (*31*). The transition state formed by TvPNP is, therefore, likely to have no significant bond order to the leaving group, similar to human PNP. Like TvPNP, human PNP also shows higher affinity for DADMe-Immucillins than for the Immucillins. An exception for TvPNP is the transition state analogues of guanosine. Guanosine has a 10-fold lower catalytic efficiency than adenosine for TvPNP, and DADMe-ImmG (**6**) and ImmG (**4**) exhibit dissociation constants of 18 and 9.4 nM, respectively. This pattern suggests that the phosphorolysis of guanosine may have an earlier transition state than that for adenosine.

The poor use of pNPR as a substrate by TvPNP is an indication that much of the catalytic potential for this enzyme arises from leaving group interactions (*32*). The tight binding of DADMe-ImmA to TvPNP is explained in the crystal structure of TvPNP·DADMe-ImmA·PO_4, where Asp204

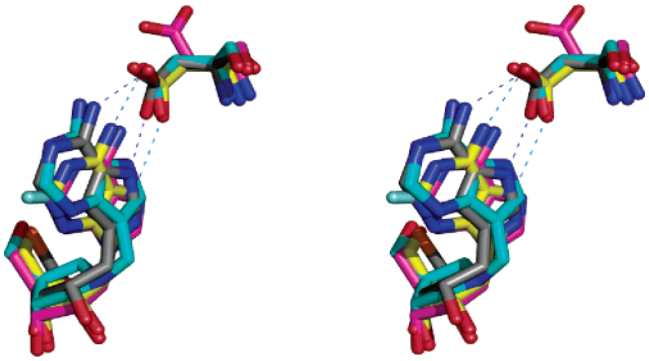

FIGURE 6: Stereoview overlay of the active site complexes of TvPNP·ImmA·PO_4 in gray (pdb ID number 2I4T), TvPNP·DADMe-ImmA·PO_4 in cyan (pdb ID number 2ISC), TvPNP·Formycin-A (1z36.pdb) in yellow, and TvPNP·2-fluoroadenosine (1z35.pdb) (*3*) in yellow. Asp204 has closer interactions with DADMe-ImmA and ImmA than with the other two TvPNP complexes.

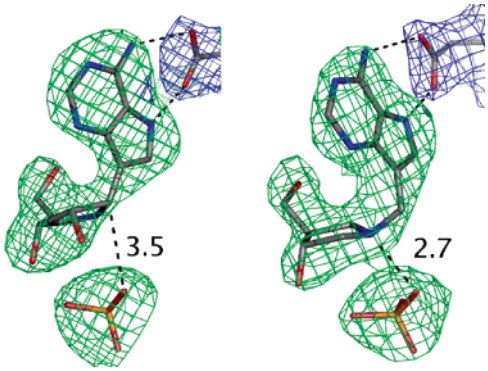

FIGURE 7: Omit maps for ImmA and phosphate contoured at 3σ around the inhibitors (green) and the 2*Fo*-*Fc* map contoured at 1σ around Asp204 (in blue) are shown on the left. The right panel is the same analysis for the complex with DADMe-ImmA. The distances between the C1′ of ImmA (left) and the N1′ of DADMe-ImmA (right) and the phosphate groups are shown in angstroms.

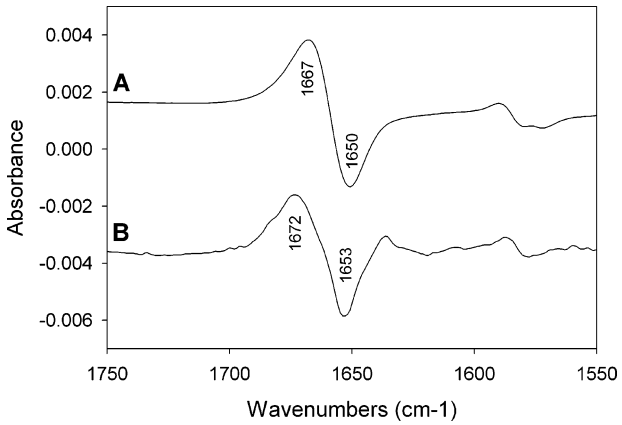

FIGURE 8: (A) Difference FTIR spectra of [6-O^{16}]ImmH (**1**) and [6-O^{18}]ImmH in solution. (B) Difference FTIR spectra of TvPNP·[6-O^{18}]ImmH·PO_4 and TvPNP·[6-O^{16}]ImmH·PO_4 complexes. Spectra with and without the added 50 mM phosphate buffer gave the same result.

forms strong hydrogen bonds with the deazaadenine group, and a 2.9 Å ion pair is formed between the phosphate anion and the N1′ cation. The unique substrate specificity of TvPNP has permitted the design of a powerful and specific transition state analogue for this unusual and specific isozyme of the PNP family.

ACKNOWLEDGMENT

We thank Dr. James Errey for valuable discussions. We thank the staff at NSLS Brookhaven National Lab for technical assistance at X29A.

REFERENCES

1. Radonjic, I. V., Dzamic, A. M., Mitrovic, S. M., Arsic, Arsenijevic, V. S., Popadic, D. M., and Kranjcic, Zec, I. F. (2005) Diagnosis of *Trichomonas vaginalis* infection: The sensitivities and specificities of microscopy, culture and PCR assay, *Eur. J. Obstet. Gynecol. Reprod. Biol. 126*, 116−120.
2. Gero, A. M., Kang, E. W., Harvey, J. E., Schofield, P. J., Clinch, K., and Furneaux, R. H. (2000) *Trichomonas vaginalis*: detection of nucleoside hydrolase activity as a potential screening procedure, *Exp. Parasitol. 94*, 125−128.
3. Zang, Y., Wang, W.-H., Wu, S.-W., Ealick, S. E., and Wang, C. C. (2005) Identification of a subversive substrate of *Trichomonas vaginalis* purine nucleoside phosphorylase and the crystal structure of the enzyme-substrate complex, *J. Biol. Chem. 280*, 22318−22325.
4. Brown, D. M., Upcroft, J. A., Dodd, H. N., Chen, N., and Upcroft, P. (1999) Alternative 2-keto acid oxidoreductase activities in *Trichomonas vaginalis*, *Mol. Biochem. Parasitol. 98*, 203−214.
5. de Koning, H. P., Bridges, D. J., and Burchmore, R. J. S. (2005) Purine and pyrimidine transport in pathogenic protozoa: From biology to therapy, *FEMS Microbiol. Rev. 29*, 987−1020.
6. Stoeckler, J. D. (1984) Purine Nucleoside Phosphorylase: A Target for Chemotherapy, in *Development in Cancer Chemotherapy* (Glazer, R. I., Ed.) pp 35−60, CRC Press, Inc., Boca Raton, FL.
7. Montgomery, J. A. (1993) Purine nucleoside phosphorylase: a target for drug design, *Med. Res. Rev. 13*, 209−228.
8. Bzowska, A., Kulikowska, E., and Shugar, D. (2000) Purine nucleoside phosphorylase: properties, functions and clinical aspects, *Pharmacol. Ther. 88*, 349−425.
9. Koellner, G., Bzowska, A., Wielgus-Kutrowska, B., Luic, M., Steiner, T., Saenger, W., and Stepinski, J. (2002) Open and closed conformation of the *E. coli* purine nucleoside phosphorylase active center and implications for the catalytic mechanism, *J. Mol. Biol. 315*, 351−371.
10. Mazella, L. J., Parkin, D. W., Tyler, P. C., Furneaux, R. H., and Schramm, V. L. (1996) Mechanistic diagnosis of N-ribohydrolases and purine nucleoside phosphorylase, *J. Am. Chem. Soc. 118*, 2111−2112.
11. Singh, V., and Schramm, V. L. (2006) Transition state structure of human 5′-methylthioadenosine phosphorylase, *J. Am. Chem. Soc. 128*, 14691−14696.
12. Handlon, A. L., Xu, C., Muller-Steffner, H. M., Schuber, F., and Oppenheimer, N. J. (1994) 2′-Ribose substituent effects on the chemical and enzymatic hydrolysis of NAD+, *J. Am. Chem. Soc. 116*, 12087−12088.
13. Rosenburg, S., and Kirsch, J. F. (1981) Oxygen-18 leaving group kinetic isotope effects on the hydrolysis of nitrophenyl glycosides. 2. Lysozyme and β-glucosidase: acid and alkaline hydrolysis, *Biochemistry 20*, 3196−3207.
14. Lewandowicz, A., Taylor, Ringia, E., Ting, L. M., Kim, K., Tyler, P. C., Evans, G. B., Zubkova, O. V., Mee, S., Painter, G. F., Lenz, D. H., Furneaux, R. H., and Schramm, V. L. (2005) Energetic mapping of transition state analogue interactions with human and plasmodium falciparum purine nucleoside phosphorylases, *J. Biol. Chem. 280*, 30320−30328.
15. Mungagala, N. R., and Wang, C. C. (2003) Adenosine is a primary precursor of all purine nucletides in *Trichomonas vaginalis*, *Mol. Biochem. Parasitol. 127*, 143−149.
16. Mungagala, N. R., and Wang, C. C. (2002) The purine nucleoside phosphorylase from *Trichomonas vaginalis* is a homologue of the bacterial enzyme, *Biochemistry 41*, 10382−10389.
17. Kim, B. K., Cha, S., and Parks, R. E., Jr. (1968) Purine nucleoside phosphorylase from human erythroyctes. II. Kinetic analysis and substrate-binding studies, *J. Biol. Chem. 243*, 1771−1776.
18. Kicska, G. A., Tyler, P. C., Evans, G. B., Furneaux, R. H., Kim, K., and Schramm, V. L. (2002) Transition state analogue inhibitors of purine nucleoside phosphorylase from *Plasmodium falciparum*, *J. Biol. Chem. 277*, 3219−3225.
19. Singh, V., Evans, G. B., Lenz, D. H., Mason, J. M., Clinch, K., Mee, S., Painter, G. F., Tyler, P. C., Furneaux, R. H., Lee, J. E., Howell, P. L., and Schramm, V. L. (2005) Femtomolar transition

state analogue inhibitors of 5′-methylthioadenosine/S-adenosylhomocysteine nucleosidase from *Escherichia coli*, *J. Biol. Chem. 280*, 18265−18273.
20. Miles, R. W., Tyler, P. C., Furneaux, R. H., Bagdassarian, C. K., and Schramm, V. L. (1998) One-third-the-sites transition-state inhibitors for purine nucleoside phosphorylase, *Biochemistry 37*, 8615 -8621.
21. Otwinowski, Z., and Minor, W. (1997) Processing of X-ray diffraction data collected in oscillation mode, *Methods Enzymol. 276*, 307−326.
22. Vagin, A., and Teplyakov, A. (1997) MOLREP: an automated program for molecular replacement, *J. Appl. Crystallogr. 30*, 1022−1025.
23. Murshudov, G. N., Vagin, A. A., and Dodson, E. J. (1997) Refinement of macromolecular structures by the maximum-likelihood method, *Acta Crystallogr., Sect. D 53*, 240−255.
24. Potterton, E., Briggs, P., Turkenburg, M., and Dodson, E. (2003) A graphical user interface to the CCP4 program suite, *Acta Crystallogr., Sect. D 59*, 1131−1137.
25. Emsley, P., and Cowtan, K. (2004) Model-building tools for molecular graphics, *Acta Crystallogr., Sect. D 60*, 2126−2132.
26. DeLano, W. L. (2002) The PyMOL Molecular Graphics System, DeLano Scientific, San Carlos, CA.
27. Kicska, G. A., Tyler, P. C., Evans, G. B., Furneaux, R. H., Schramm, V. L., and Kim, K. (2002) Purine-less death in *Plasmodium falciparum* induced by Immucillin-H, a transition state analogue of purine nucleoside phosphorylase, *J. Biol. Chem. 277*, 3226−3231.
28. Kicska, G. A., Tyler, P. C., Evans, G. B., Furneaux, R. H., Shi, W., Fedorov, A., Lewandowicz, A., Cahill, S. M., Almo, S. C., and Schramm, V. L. (2002) Atomic dissection of the hydrogen bond network for transition-state analogue binding to purine nucleoside phosphorylase, *Biochemistry 41*, 14489−14498.
29. Ting, L. M., Shi, W., Lewandovicz, A., Singh, V., Mwakingwe, A., Birck, M. R., Ringia, E. A., Bench, G., Madrid, D. C., Tyler, P. C., Evans, G. B., Furneaux, R. H., and Schramm, V. L. (2005) Targetign a novel *Plasmodium falciparum* purine recycling pathway with specific immucillins, *J. Biol. Chem. 280*, 9547−9554.
30. Bennett, E. M., Li, C., Allan, P. W., Parker, W. B., and Ealick, S. E. (2003) Structural basis for substrate specificity of *E. coli* purine nucleoside phosphorylase, *J. Biol. Chem. 278*, 47110−47118.
31. Taylor Ringia, E. A., Tyler, P. C., Evans, G. B., Furneaux, R. H., Murkin, A. S., and Schramm, V. L. (2006) Transition state analogue discrimination by related purine nucleoside phosphorylases, *J. Am. Chem. Soc. 128*, 7126−7127.
32. Schramm, V. L. (2003) Enzymatic transition state poise and transition state analogues, *Acc. Chem. Res. 36*, 588−596.

BI061515R